CARDIFF UNIVERSITY
PRIFYSGOL CAERDYDD

ORCA – Online Research @ Cardiff

This is an Open Access document downloaded from ORCA, Cardiff University's institutional repository:https://orca.cardiff.ac.uk/id/eprint/110239/

This is the author's version of a work that was submitted to / accepted for publication.

Citation for final published version:

Nowicka, Ewa , Reece, Christian, Althahban, Sultan M., Mohammed, Khaled M. H., Kondrat, Simon A., Morgan, David J. , He, Qian , Willock, David J. , Golunski, Stanislaw , Kiely, Christopher J. and Hutchings, Graham J. 2018. Elucidating the role of CO2 in the soft oxidative dehydrogenation of propane over ceria-based catalysts. ACS Catalysis 8 , pp. 3454-3468. 10.1021/acscatal.7b03805

Publishers page: http://dx.doi.org/10.1021/acscatal.7b03805

Please note:
Changes made as a result of publishing processes such as copy-editing, formatting and page numbers may not be reflected in this version. For the definitive version of this publication, please refer to the published source. You are advised to consult the publisher's version if you wish to cite this paper.

This version is being made available in accordance with publisher policies. See http://orca.cf.ac.uk/policies.html for usage policies. Copyright and moral rights for publications made available in ORCA are retained by the copyright holders.

Supporting Information

Elucidating the role of CO_2 in the soft oxidative dehydrogenation of propane over ceria-based catalysts

Ewa Nowicka,[a,b*] Christian Reece,[a] Sultan M. Althahban,[c] Khaled Mohammed [d,e,f] Simon A. Kondrat,[a,g] David J. Morgan,[a] Qian He,[a] David J. Willock,[a] Stanislaw Golunski,[a] Christopher J. Kiely [a,c] and Graham J. Hutchings[a*]

[a] *School of Chemistry, Cardiff University, Main Building, Park Place, Cardiff, CF10 3AT, UK*

[b] *Institut für Chemie, Technische Universität Berlin, Straße des 17. Juni 124, 10623 Berlin, Germany*

[c] *Department of Materials Science and Engineering, Lehigh University, 5 East Packer Avenue, Bethlehem, PA 18015-3195, USA*

[d] *Chemistry Department, Faculty of Science, Sohag University, Sohag, 82524, Egypt*

[e] *UK Catalysis Hub, Research Complex at Harwell, RAL, Harwell, OX110FA, Oxfordshire, UK.*

[f] *Department of Chemistry, University College London, 20 Gordon Street, London WC1H 0AJ, UK*

[g] *Department of Chemistry, Loughborough University, Loughborough, Leicestershire, LE11 3TU, UK*

*****Correspondence to Graham J. Hutchings, e-mail: hutch@cardiff.ac.uk and Ewa Nowicka, e-mail: nowickae@cardiff.ac.uk

List of sections, tables and figures:

Catalytic performance calculations.

Temperature programmed reduction: simulation of experimental data.

Tables

Table S1. Propane conversion and selectivity of Pd over various Ce-based catalyst formulations.

Table S2. Zr K-edge derived k3-weighed EXAFS fitting parameters.

Figures

Figure S1. Comparison of conversion (filled symbols) and selectivity (empty symbols) between Pd/CeZrAlO$_x$ (■) and CeZrAlO$_x$ (●) *Reaction conditions:* GHSV=6000 h^{-1}, T=500 °C, 37% C_3H_8, 37% CO_2, 26% He.

Figure S2. Selectivity of products in the thermal dehydrogenation reaction. *Reaction conditions:* 37% C_3H_8, 67% He; GHSV=6000 h^{-1}, T=500 °C. *Legend:* ■:C_3H_6, ▲:CH_4, ▼:C_2H_4, ●: CO_x, □: carbon balance

Figure S3. Conversion of C_3H_8 (■) and CO_2 (●) during subsequent oxidative dehydrogenation (37% C_3H_8, 37% CO_2, 26% He) along with CO_2: CO balance. Reaction conditions: GHSV=6000 h^{-1}, T=500 °C.

Figure S4. Zr K-edge derived k3-weighted EXAFS data (left column) and magnitudes of Fourier-transformed data (right column) from A) CeZrAlO$_x$, B) fresh Pd-CeZrAlO$_x$ and C) 4 h used Pd-CeZrAlO$_x$, D) tetragonal ZrO_2 and E) monoclinic ZrO_2.

Figure S5. Zr K-edge XANES of CeZrAlO$_x$ support compared with a tetragonal ZrO_2 standard

Figure S6. Pd K-edge derived k3-weighted EXAFS data (left column) and magnitudes of Fourier-transformed data (right column) for a, b) fresh 5%Pd/CeZrAlO$_x$: c, d) 4 h used 5%Pd/CeZrAlO$_x$; e, f) 140 h used 5%Pd/CeZrAlO$_x$.

Figure S7. XPS spectra for the Ce(3d) region for the various 5%Pd/CeZrAlO$_x$ catalysts, fitted with line-shapes for Ce(IV) and Ce(III) species.

Figure S8. TPD profiles of 5%Pd/CeZrAlO$_x$ material using different gases: A) NH_3 and B) CO_2.

Figure S9. SEM-XEDS mapping data obtained on the 5%Pd/CeZrAlO$_x$ catalyst showing the excellent homogeneity of Ce, Zr and Al distribution compared to that of Pd.

Figure S10. Raman analysis of the CeZrAlO$_x$ support. The and at 620 cm^{-1} is clear evidence of the presence of a pseudo-cubic, tetragonal Ce–Zr phase.

Figure S11. DRIFT analysis of the calcined $CeZrAlO_x$ support a) when fresh, b) under N_2 flow and c) under CO_2 flow.

Figure S12. TGA analysis of the fresh and used 5wt%Pd/$CeZrAlO_x$ catalysts.

Catalytic performance calculations:

Propane conversion X, was calculated as follows

$$X = \left(1 - \frac{F_{C3H8_{out}}}{F_{C3H8_{in}}}\right) * 100\%$$

Where: $F_{C3H8out}$ = flow of propane out of the reactor

F_{C3H8in} = flow of propane into the reactor

$$S = \left(\frac{F_{A,out}}{\sum F_{carbon\ prod}}\right) * 100\%$$

Where: $F_{A,out}$ = flow of carbon in product A out of reactor (*)

$F_{\text{carbon prod}}$ = flow of all carbon from products* out of reactor

** products excluding carbon oxides*

Table S1. Propane conversion and selectivity of Pd over various Ce based catalyst formulations.

Reaction conditions: 37% C_3H_8, 37% CO_2, 26% He; GHSV=6000 h^{-1}, T = 500 °C

Pd loading (%)	**Support composition**	**Conversion (%)***	**Selectivity (%)***
5	$Ce_{0.33}Zr_{0.33}Al_{0.33}O_x$	10.2	90
	$Ce_{0.25}Zr_{0.25}Al_{0.5}O_x$	9.5	93
	$Ce_{0.16}Zr_{0.33}Al_{0.5}O_x$	9.2	80
	$Ce_{0.157}Zr_{0.157}Al_{0.66}O_x$	9.3	91
0.1	$Ce_{0.25}Zr_{0.25}Al_{0.5}O_x$	3.1	90
0.5		3.6	92
2.5		6.5	92
7.5		13.2	69
10		5.8	31

*Measured after 1 h of stream

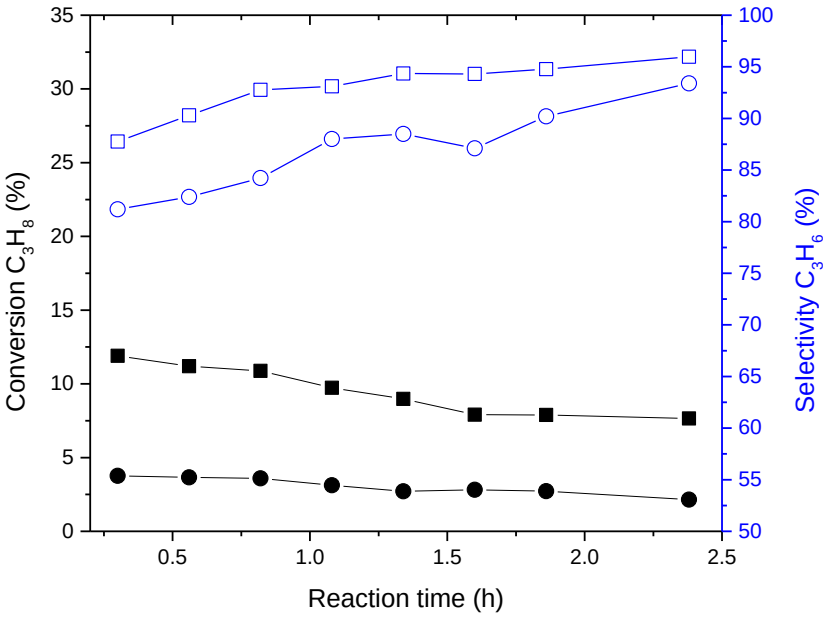

Figure S1. Comparison of conversion (filled symbols) and selectivity (empty symbols) between Pd/CeZrAlO$_x$ (■) and CeZrAlO$_x$ (●) *Reaction conditions:* GHSV=6000 h^{-1}, T=500 °C, 37% C_3H_8, 37% CO_2, 26% He.

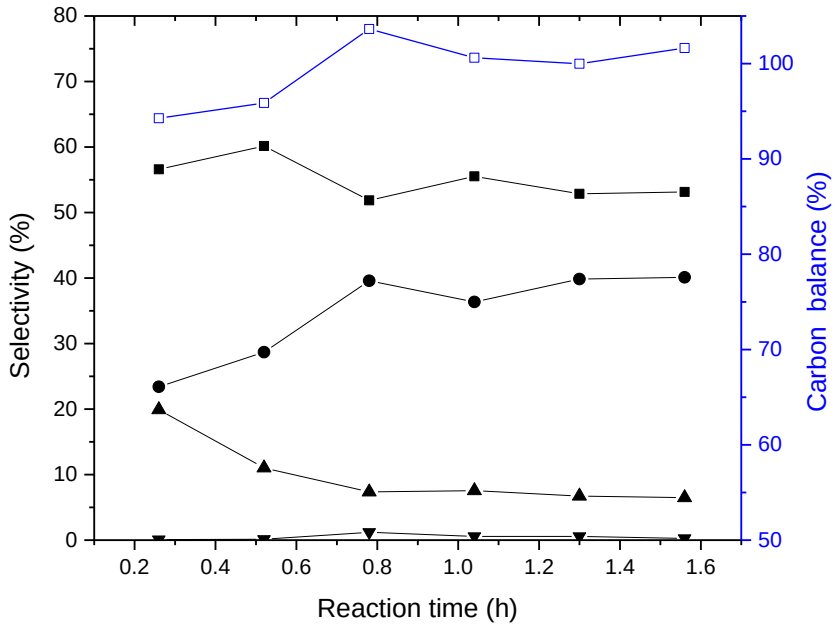

Figure S2. Selectivity of products in the thermal dehydrogenation reaction. *Reaction conditions:* 37% C_3H_8, 67% He; GHSV=6000 h^{-1}, T=500 °C. *Legend:* ■:C_3H_6, ▲:CH_4, ▼:C_2H_4, ●: CO_x, □: carbon balance.

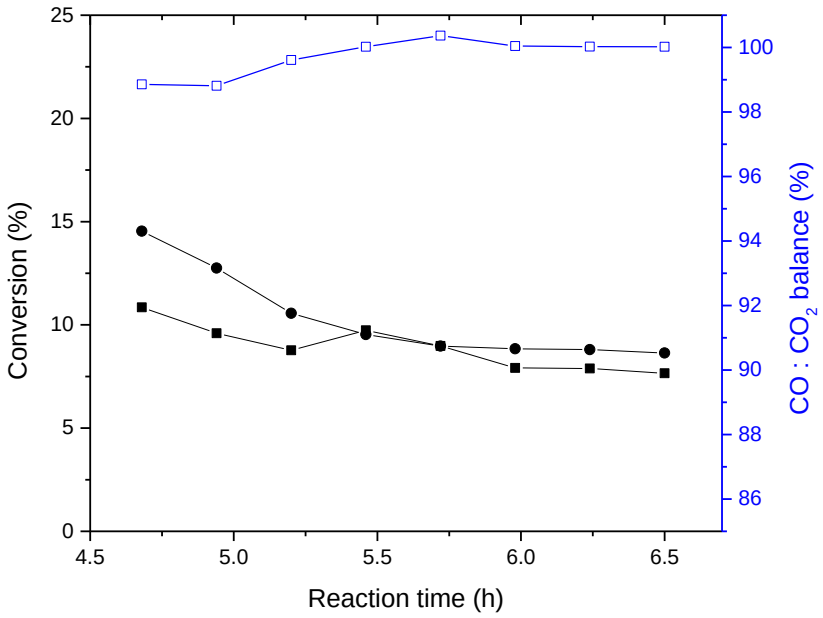

Figure S3. Conversion of C_3H_8 (■) and CO_2 (●) during subsequent oxidative dehydrogenation (37% C_3H_8, 37% CO_2, 26% He) along with CO_2: CO balance. *Reaction conditions:* GHSV=6000 h^{-1}, T=500 °C.

Table S2. Zr K-edge derived k3-weighed EXAFS fitting parameters.

Material	**bond**	**N**	**σ^2 (Å^2)**	**r (Å)**	**ΔE_0 (eV)**	**R-factor**
$CeZrAlO_x$	Zr-O1	3.2 (7)	0.0019	2.121 (8)	2.385	0.0079
	Zr-O2	2.3 (3)	0.0019	2.275 (14)		
Pd-$CeZrAlO_x$ fresh	Zr-O1	2.9 (5)	0.0007	2.120 (9)	1.646	0.0155
	Zr-O2	2.2 (2)	0.0007	2.276 (14)		
$PdCeZrAlO_x$4h used	Zr-O1	3.1 (7)	0.0014	2.126 (10)	2.454	0.0172
	Zr-O2	2.2 (3)	0.0014	2.284 (17)		
Tetragonal ZrO_2	Zr-O1	3.5(8)	0.0041	2.137 (22)	2.802	0.0361
	Zr-O2	2.3(7)	0.0041	2.352 (38)		
Monoclinic ZrO_2	Zr-O1	2.7(6)	0.0016	2.126 (24)	2.144	0.0217
	Zr-O2	2.7(5)	0.0016	2.272 (26)		

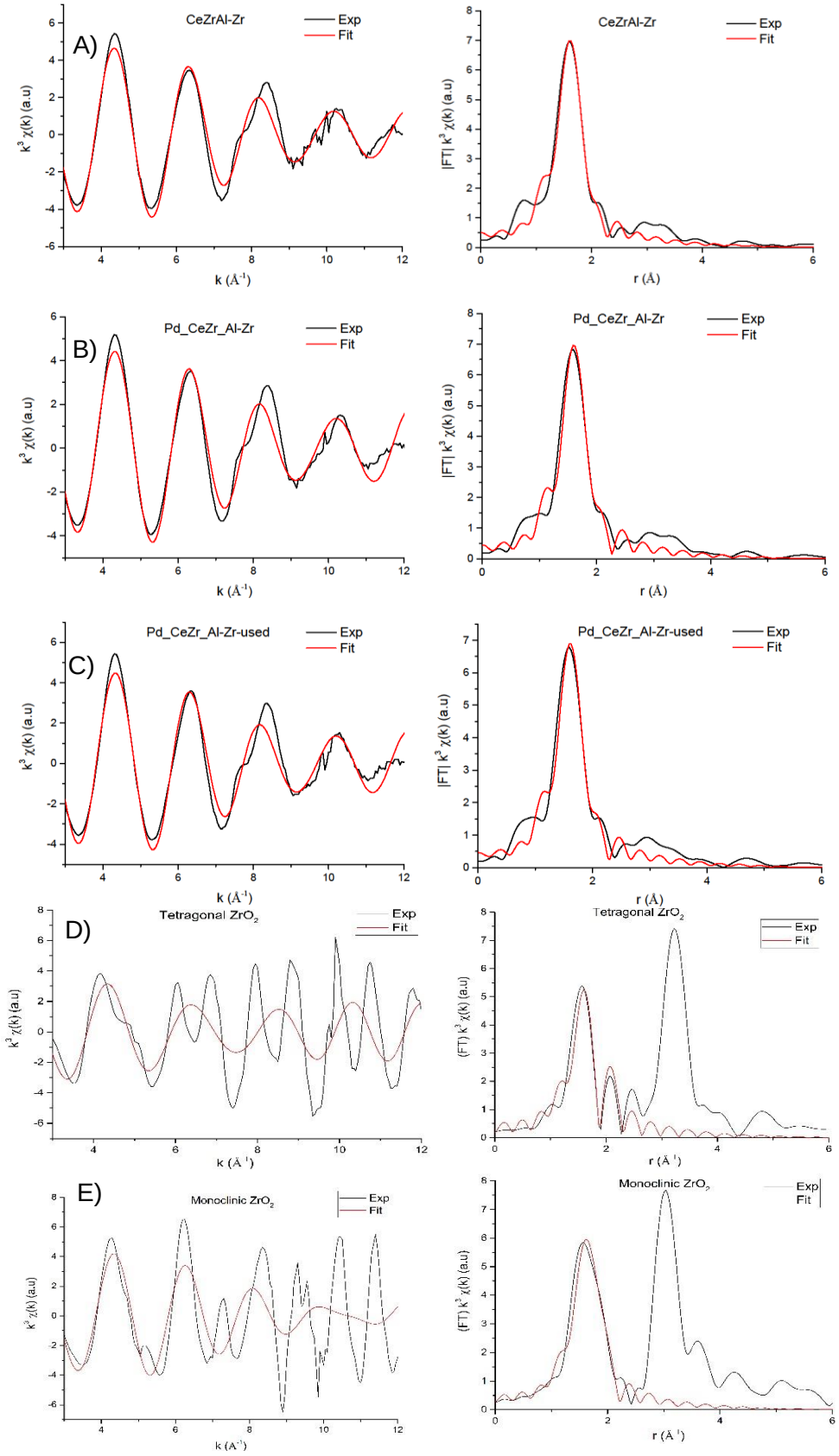

Figure S4. Zr K-edge derived k3-weighted EXAFS data (*left column*) and magnitudes of Fourier-transformed data (*right column*) from A) $CeZrAlO_x$, B) fresh Pd-$CeZrAlO_x$, C) 4 h used Pd-$CeZrAlO_x$, D) tetragonal ZrO_2 and E) monoclinic ZrO_2.

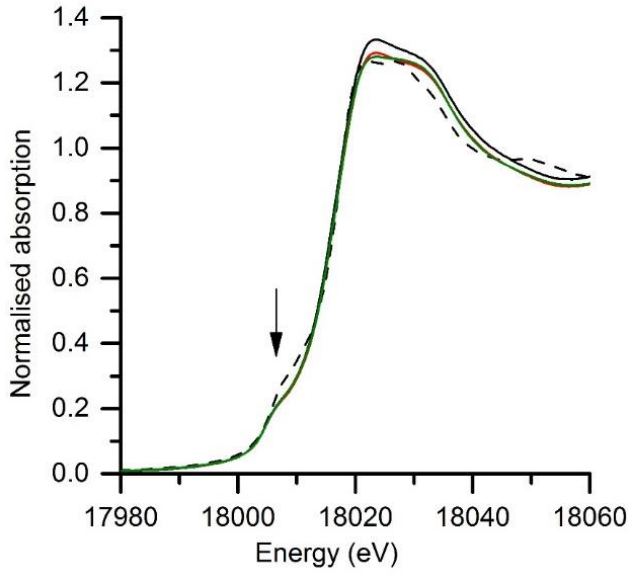

Figure S5. Zr K-edge XANES of $CeZrAlO_x$ support compared with a tetragonal ZrO_2 standard.

Key: Dashed black line: tetragonal ZrO_2; black solid line: $CeZrAlO_x$; red solid line: fresh $Pd/CeZrAlO_x$; and green solid line: 4 h used $Pd/CeZrAlO_x$. The arrow indicates the position of the 1s to 4d pre-edge transition.

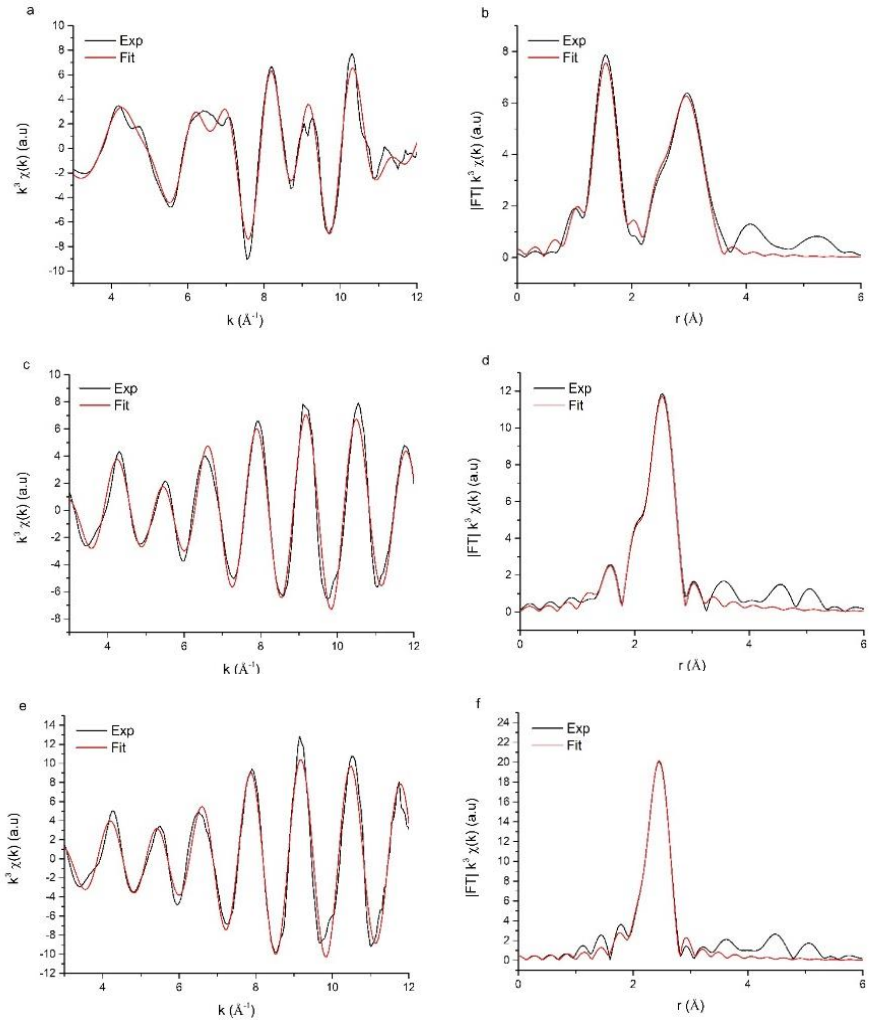

Figure S6. Pd K-edge derived k3-weighted EXAFS data (left column) and magnitudes of Fourier-transformed data (right column) for a, b) fresh 5%Pd/CeZrAlO$_x$: c, d) 4 h used 5%Pd/CeZrAlO$_x$; e, f) 140 h used 5%Pd/CeZrAlO$_x$.

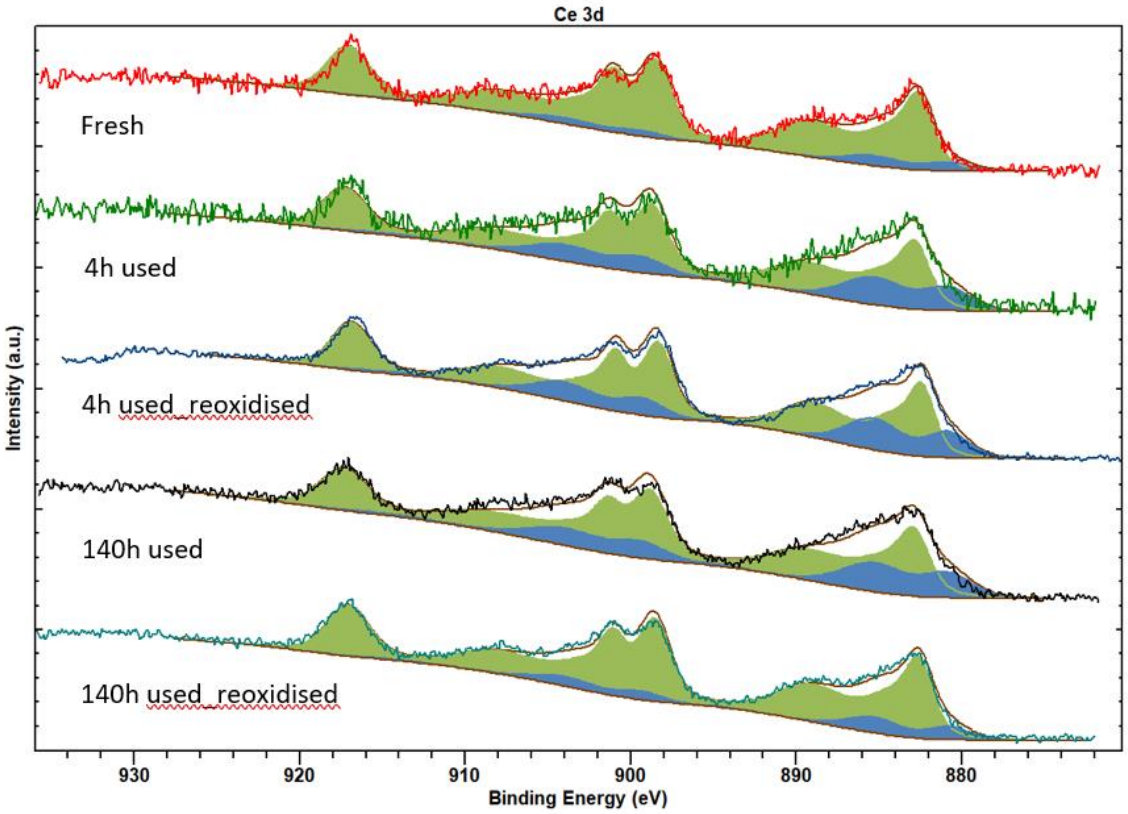

Figure S7. XPS spectra for the Ce(3d) region for the various 5%Pd/CeZrAlO_x catalysts, fitted with line-shapes for Ce(IV) and Ce(III) species.

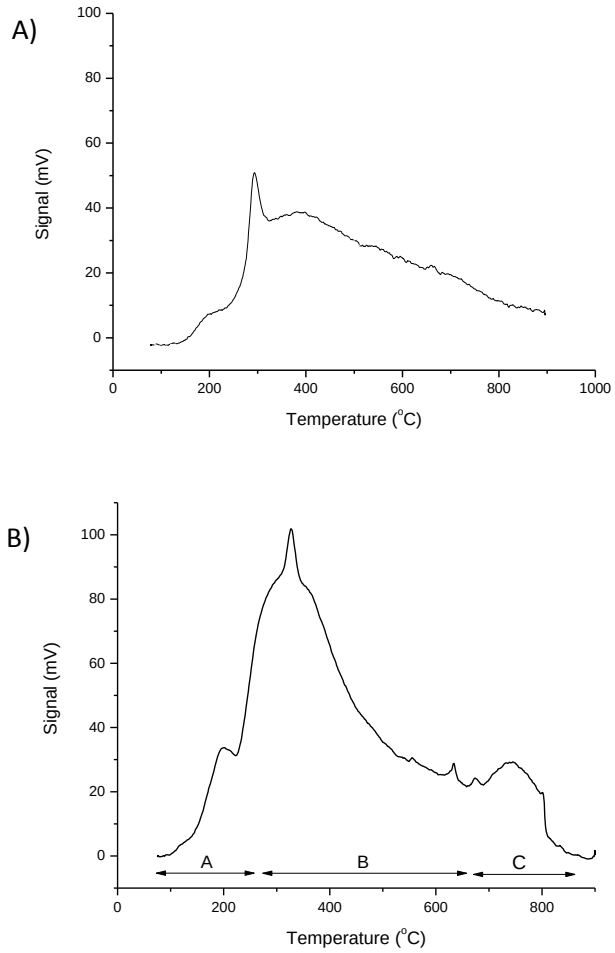

Figure S8. TPD profiles of 5%Pd/CeZrAlO_x material using different gases: A) NH_3 and B) CO_2.

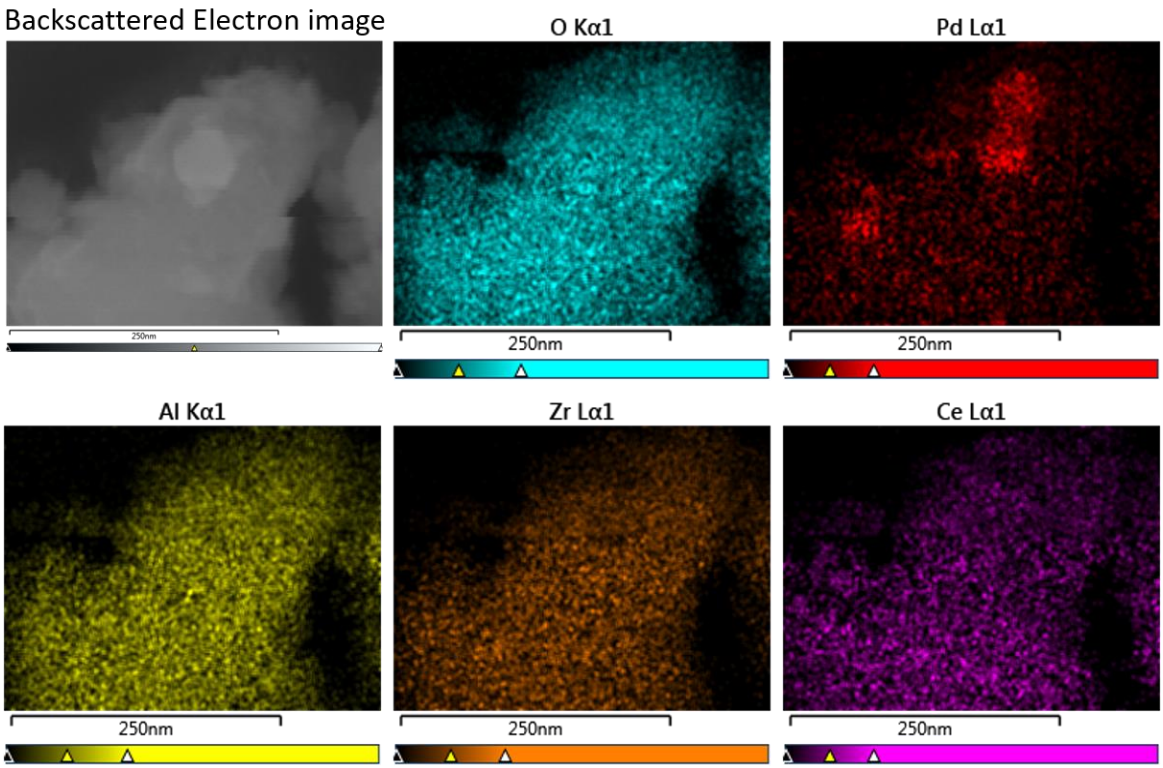

Figure S9. ***Additional*** SEM-XEDS mapping data obtained on the 5%Pd/CeZrAlO_x catalyst showing the excellent homogeneity of Ce, Zr and Al distribution compared to that of Pd.

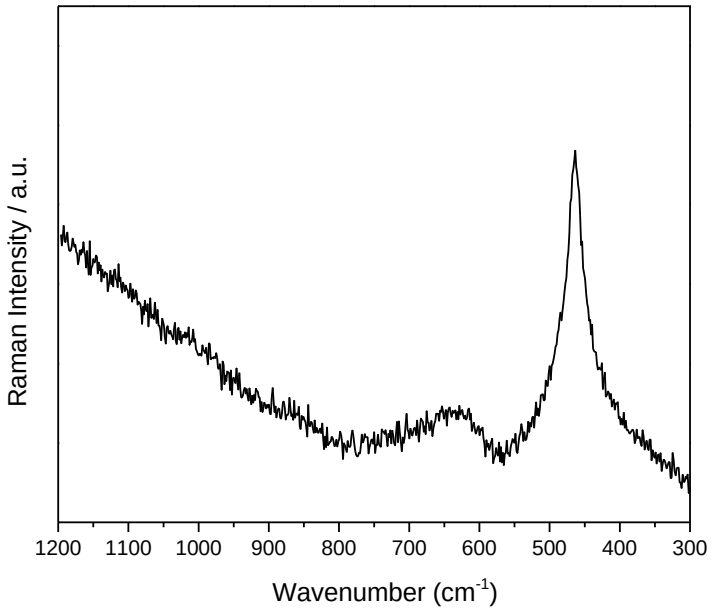

Figure S10. Raman analysis of $CeZrAlO_x$ support. The band at 620 cm^{-1} is clear evidence of the presence of a pseudo-cubic, tetragonal Ce–Zr phase.[1]

Temperature programmed reduction: simulation of experimental data

Temperature programmed reduction experiments primarily characterise the rate of specific processes that can be thermally stimulated. The rate can be parameterised very simply as a function of temperature T and the extent of the process α (which varies from 0 at the beginning to 1 when completed).

$$\frac{d\alpha}{dt} = k(T)f(\alpha)$$

The pressure of the reactant gas is also a factor in this experiment, but for the purposes of our work it can be ignored as the reactant gases are kept in excess and can be assumed to be constant. The temperature dependence of the rate k(T) can be parameterised using the Arrhenius equation.

$$\frac{d\alpha}{dt} = A \exp\left(\frac{-E_a}{RT}\right) f(\alpha)$$

with A being the Arrhenius pre-exponential factor, E_a the activation energy, R the gas constant and T the temperature. This expression assumes a constant activation energy over the entire process α. In order to correct for any change in E_a as the material becomes more reduced, an extra parameter γ can be included in the equation.

$$\frac{d\alpha}{dt} = A \exp\left(\frac{-E_a(1+\gamma\alpha)}{RT}\right) f(\alpha)$$

The parameter γ describes a linear relationship between the E_a and α. A positive value of γ indicates an increase in the distance between the active site for the H_2 dissociation and reduction. The final term to be parameterised is the degree of conversion dependence of the process. It is possible to apply some simple kinetics to parameterise this dependence, but it is found for TPR experiments it is best to use a model free approach outlined by Sestak and Berggren[2] which can represent a large number of reaction models through its kinetic parameters *m*, *n*, and *p*.

$$f(\alpha) = \alpha^m(1-\alpha)^n[-\ln(1-\alpha)]^p$$

The Sestak and Berggren (SB) function is often truncated so that p = 0 as it is found that often only *m* and *n* are required to describe the TPR reduction processes. These parameters are not

derived from any specific kinetic model and therefore have no true physical meaning, but it is possible to infer information from their values. It can be seen that the shape parameter *m* is dominant at higher degrees of reduction, whereas *n* is dominant at lower degrees of reduction. For a temperature programmed reduction experiment the relative magnitude of these two parameters can be linked to the influence of the reduced and oxidised material respectively on the shape (which described the kinetics) of the reduction profile (e.g., a higher relative *m* value indicates the shape is more dominated by the reduced material, and a higher relative *n* value indicates the shape is dominated by the oxidised material). In the past there has been some work to attempt to link these parameters to specific processes occurring during a TPR experiment with moderate success.[3] Finally, for temperature programmed experiments, time can be directly related to the temperature through the following relationship.

$$\frac{d\alpha}{dt} = \beta \frac{d\alpha}{dT}$$

with β being the heating rate of the experiment, the final form of the function can then be expressed using

$$\frac{d\alpha}{dT} = \frac{A}{\beta} \exp\left(\frac{E_a(1+\gamma\alpha)}{RT}\right) \alpha^m (1-\alpha)^n$$

For a complex reduction profile such as the ones measured in this paper, it becomes pertinent to express the total reduction profile as a simple sum of individual processes, such that

$$\frac{d\alpha}{dT} = \sum_{N=1}^{N} \frac{d\alpha_N}{dT}$$

with N being the number of individual reduction processes which make up the total profile. As one can imagine as you increase N, the goodness of overall fit to the experimental thermogram will increase, therefore for this work a value of N was selected to the minimum value which would still enable us to describe the major features of the thermogram, while also making sense physically.

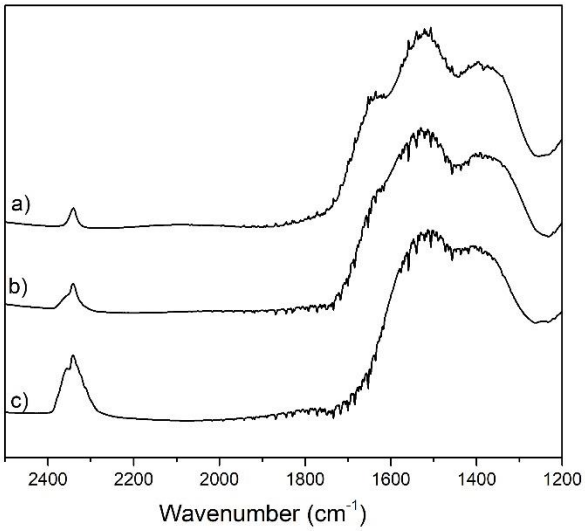

Figure S11. DRIFT analysis of calcined $CeZrAlO_x$ support a) when fresh, b) under N_2 flow and c) under CO_2 flow.

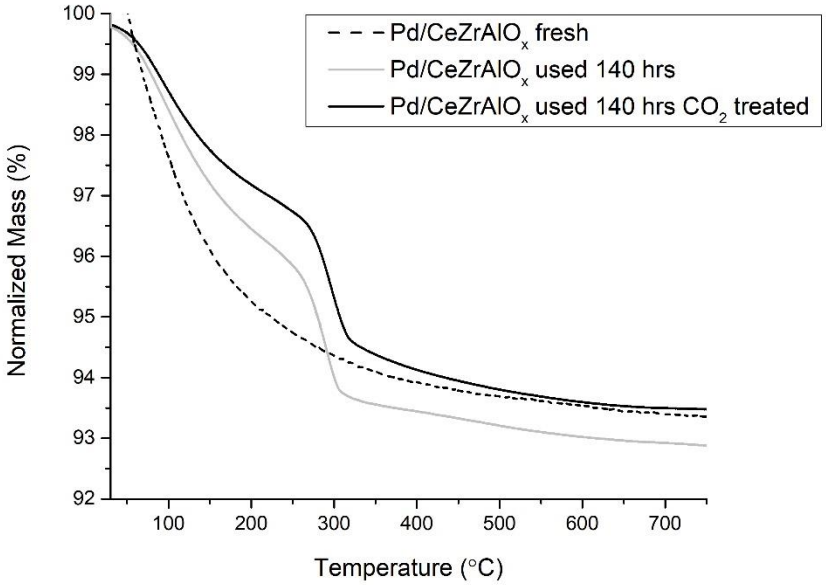

Figure S12. TGA analysis of the fresh and used 5wt%$Pd/CeZrAlO_x$ catalysts.

References:

1. Lan, L.; Chen, S.; Cao, Y.; Gong, M.; Chen, Y., New insights into the structure of a CeO_2-ZrO_2-Al_2O_3 composite and its influence on the performance of the supported Pd-only three-way catalyst. *Catal. Sci. Tech.* **2015,** *5*, 4488-4500.

2. Šesták, J.; Berggren, G., Study of the kinetics of the mechanism of solid-state reactions at increasing temperatures. *Thermochim. Acta* **1971,** *3*, 1-12.

3. Munteanu, G.; Ilieva, L.; Nedyalkova, R.; Andreeva, D., Influence of gold on the reduction behaviour of Au–V_2O_5/CeO_2 catalytic systems: TPR and kinetic parameters of reduction. *Appl. Catal. A: Gen.* **2004,** *277*, 31-40.